Nuclear Lattice Effective Field Theory: Status and Perspectives

U.-G. Meißner for the NLEFT Collaboration

published in

NIC Symposium 2020
M. Müller, K. Binder, A. Trautmann (Editors)

Forschungszentrum Jülich GmbH,
John von Neumann Institute for Computing (NIC),
Schriften des Forschungszentrums Jülich, NIC Series, Vol. 50,
ISBN 978-3-95806-443-0, pp. 161.
http://hdl.handle.net/2128/24435

Nuclear Lattice Effective Field Theory: Status and Perspectives

Ulf-G. Meißner[1,2,3]
for the NLEFT Collaboration

[1] Helmholtz-Institut für Strahlen- und Kernphysik and Bethe Center for Theoretical Physics, Universität Bonn, 53115 Bonn, Germany
E-mail: meissner@hiskp.uni-bonn.de

[2] Institute for Advanced Simulation (IAS-4), Institut für Kernphysik (IKP-3) and Jülich Center for Hadron Physics, Forschungszentrum Jülich, 52425 Jülich, Germany

[3] Tbilisi State University, 0186 Tbilisi, Georgia

I give an outline of the recent developments in nuclear lattice effective field theory, which is continuing to push the boundaries of *ab initio* nuclear many-body calculations, both in terms of nuclear structure and nuclear reactions. This remarkable progress has been made possible by recent dramatic increases in HPC resources, as well as advances in computational methods and algorithmic developments.

1 Introduction

Recent advances in high-performance computing (HPC) have enabled nuclear physics to enter a new and exciting era. Calculations of nuclear structure and reactions that were once considered nearly impossible are now being readily performed. The research performed by the NLEFT (Nuclear Lattice Effective Field Theory) collaboration is at the forefront of this development. Such calculations are *ab initio* in the sense that they use nuclear forces derived from the chiral effective Lagrangian of Quantum Chromodynamics (QCD), which is the underlying theory that describes the interactions of quarks and gluons. For few-nucleon systems, the chiral effective field theory (EFT) for the forces between two, three and four nucleons have been worked out to high orders in the chiral power counting, see *e. g.* Ref. 1. This force consists of long-ranged exchanges of one or more pions, and shorter-ranged multi-nucleon contact interactions. By combining these EFT forces with Monte Carlo methods developed by the lattice QCD community, the NLEFT collaboration has successfully studied the properties of p-shell nuclei (such as ^{12}C and ^{16}O). These nuclei have formed the calculational boundary of more traditional nuclear many-body techniques, such as Green's function Monte Carlo.

With recent advances in the methods and algorithms of NLEFT, this boundary has been pushed further by recent *ab initio* calculations of nuclei in the sd-shell and beyond. Furthermore, the NLEFT formalism has been developed and adapted to include the treatment of nuclear reactions. This ongoing line of research is now rapidly addressing key questions related to the formation of elements, including those that enable life as we know it. In the following, we briefly review the motivation and methodology behind the NLEFT formalism. We also present recent highlights of our research and conclude with an outlook on future progress.

2 Theoretical Background of NLEFT Simulations

Nuclei are self-bound systems of nucleons (protons and neutrons). As the nucleons themselves consist of quarks and gluons, and hence are not fundamental degrees of freedom, the forces between nucleons are not completely given in terms of two-body interactions, but include three-body and higher order interaction terms. Computing the properties of multi-nucleon systems presents a very difficult challenge. The complicated structure of the interaction coupled with the quantum mechanical nature of such systems leads to an exponential growth in the computational effort as a function of the number of nucleons A. For $A \leq 4$, bound state energies and scattering phase shifts have traditionally been calculated by exact (numerical) solutions of the Lippmann-Schwinger or Faddeev-Yakubowsky equations. For $A \geq 5$, well established many-body techniques have been developed, such as the no-core shell model and coupled-cluster methods. These ultimately rely on the direct diagonalisation of a large matrix M in order to solve a problem of the form $Mx = b$. As the size of M increases exponentially, the memory and processing power of currently available HPC systems are quickly exhausted, which confines such methods to systems with $A \leq 12$. In order to push beyond $A = 12$, simplifications to the interaction between nucleons as well as other assumptions become necessary.

In the context of QCD, systems of quarks and gluons also exhibit exponential scaling in the number of degrees of freedom, but instead of relying on direct diagonalisation in order to calculate observables, methods have been developed to stochastically *estimate* observables. The quarks and gluons are placed on a discrete space-time lattice, and Monte Carlo sampling of the propagation of the particles is performed in order to capture the most relevant contributions to a given observable. Such "lattice QCD" calculations provide a much reduced calculational complexity. Moreover, lattice QCD calculations are fully non-perturbative and provide the only known rigorous way to compute the properties of QCD in the non-perturbative (low-energy) regime. Still, it should be kept in mind that the stochastic nature of lattice QCD induces an associated uncertainty in each calculated observable, in addition to possible issues arising from numerical sign oscillations (the "sign problem") or from an unfavourable signal-to-noise ratio, particularly when nucleons (baryons) are involved.

While a formalism similar to lattice QCD is used in NLEFT calculations, in the latter case the nucleons form the degrees of freedom that propagate on the space-time lattice, such that the interactions between nucleons are provided by chiral EFT. The stochastic nature of the Monte Carlo importance sampling of the nucleons' trajectories provides a softer scaling of computational complexity with A. This, in turn, is what allows NLEFT to push the boundaries of *ab initio* calculations beyond those reached by more traditional methods.

3 Nuclear Physics on a Space-Time Lattice

In NLEFT simulations, Euclidean space-time is discretised on a torus of volume $L_s^3 \times L_t$, where L_s is the side length of the (cubic) spatial dimension, and L_t denotes the extent of the Euclidean time dimension. The lattice spacing in the spatial dimensions is denoted a, analogously to a_t in the temporal dimension. The maximal momentum on the lattice is thus $p_{\max} \equiv \pi/a$, which serves as the UV regulator of the theory. Nucleons exist as pointlike

particles on the lattice sites, and the interactions between nucleons (pion exchanges and contact terms) are treated as insertions on the nucleon world lines via auxiliary-field representations. The nuclear forces have an approximate spin-isospin SU(4) symmetry (Wigner symmetry) that is of fundamental importance in suppressing numerical sign oscillations that plague any Monte Carlo simulation of strongly interacting fermions at finite density. This is in contrast to lattice QCD, where any finite baryon chemical potential renders the Monte Carlo simulation unfeasible.

We compute the properties of multi-nucleon systems by means of the transfer matrix projection Monte Carlo method. There, each nucleon is treated as a single particle propagating in a fluctuating background of pion and auxiliary fields, the latter representing the multi-nucleon contact interactions. Due to the very strong binding between four nucleons occupying the same lattice site, we find that the convergence of the chiral EFT expansion can be greatly accelerated by means of smeared leading-order (LO) contact interactions. We start the Euclidean time projection from a Slater determinant Ψ_A of single-nucleon standing waves for Z protons and N neutrons (with $A = Z + N$) in a periodic cube. More complicated initial states, such as α-clusters or alike, are also possible. We then use a Wigner SU(4) symmetric Hamiltonian as a computationally inexpensive filter for the first few Euclidean time steps, which also suppresses sign oscillations dramatically. Finally, we apply the full LO chiral EFT Hamiltonian and calculate the ground state energy and other properties from the correlation function

$$Z(t) \equiv \langle \Psi_A | \exp(-tH) | \Psi_A \rangle = \mathrm{Tr}\{M^{L_t}\} \tag{1}$$

in the limit of large Euclidean projection time t. M is the usual normal-ordered transfer -matrix operator and L_t is the number of Euclidean time steps. Higher-order contributions, such as the Coulomb repulsion between protons and other isospin-breaking effects (due to the light quark mass difference), are computed as perturbative corrections to the LO amplitude. The properties of excited states are obtained from a multi-channel projection Monte Carlo method. In our LO lattice action, the nucleon kinetic energy and momentum-dependent smearing factors of the contact interactions are treated using $\mathcal{O}(a^4)$ improvement. Moreover, all lattice operators are included up to $\mathcal{O}(Q^3)$, where Q denotes the momentum transfer between pions and nucleons. This includes operators related to the breaking of rotational symmetry on the lattice. The strengths of such operators can be tuned to eliminate unphysical effects, such as the mixing of the ${}^3D_3$ partial wave into the ${}^3S_1$-${}^3D_1$ channel. Similarly, the breaking of Galilean invariance in moving frames is taken care of. A much more detailed description is given in the recent monograph.[2]

4 New Algorithms and Recent NLEFT Results

We shall now discuss the highlights of selected recent NLEFT calculations, which demonstrate both the strengths of the NLEFT approach as well as recent algorithmic developments. We start with the latter.

4.1 The Pinhole Algorithm

Auxiliary-field Monte Carlo (AFMC) simulations are efficient for computing the quantum properties of systems with attractive pairing interactions. By the calculating the exact

quantum amplitude for each configuration of auxiliary fields, we obtain the full set of correlations induced by the interactions. However, the exact quantum amplitude for each auxiliary field configuration involves quantum states which are superpositions of many different centre-of-mass positions. Therefore information about density correlations relative to the centre of mass is lost. The pinhole algorithm[3] is a new computational approach that allows for the calculation of arbitrary density correlations with respect to the centre of mass. As this was not possible in all previous AFMC simulations, adaptations of this technique should have wide applications to hadronic, nuclear, condensed matter, and ultracold atomic simulations.

Let $\rho_{i,j}(\mathbf{n})$ be the density operator for nucleons with spin i and isospin j at lattice site $\mathbf{n}$,

$$\rho_{i,j}(\mathbf{n}) = a^\dagger_{i,j}(\mathbf{n}) a_{i,j}(\mathbf{n}) \tag{2}$$

We construct the normal-ordered A-body density operator

$$\rho_{i_1,j_1,\cdots i_A,j_A}(\mathbf{n}_1,\cdots \mathbf{n}_A) = :\rho_{i_1,j_1}(\mathbf{n}_1)\cdots\rho_{i_A,j_A}(\mathbf{n}_A): \tag{3}$$

In the A-nucleon subspace, we note the completeness identity

$$\sum_{i_1,j_1,\cdots i_A,j_A} \sum_{\mathbf{n}_1,\cdots \mathbf{n}_A} \rho_{i_1,j_1,\cdots i_A,j_A}(\mathbf{n}_1,\cdots \mathbf{n}_A) \; = A! \tag{4}$$

The new feature of the pinhole algorithm is that MC importance sampling is performed according to the absolute value of the expectation value

$$\langle \Psi_f | M_*^{L_t'} M^{L_t/2} \rho_{i_1,j_1,\cdots i_A,j_A}(\mathbf{n}_1,\cdots \mathbf{n}_A) M^{L_t/2} M_*^{L_t'} | \Psi_i \rangle \tag{5}$$

Here, M^t is the transfer matrix at time t of dimension $A \times A$ and M_*^t is referring to the SU(4) invariant transfer matrix used at the beginning and at the end of the time evolution to tame the sign problem, see *e. g.* Ref. 2. Due to the completeness identity Eq. (4), the sum of the amplitude in Eq. (5) over $\mathbf{n}_1,\cdots \mathbf{n}_A$ and $i_1, j_1, \cdots i_A, j_A$ gives $A!$ times the amplitude without any insertion of the A-body density,

$$\langle \Psi_f | M_*^{L_t'} M^{L_t} M_*^{L_t'} | \Psi_i \rangle \tag{6}$$

The pinhole locations $\mathbf{n}_1,\cdots \mathbf{n}_A$ and spin-isospin indices $i_1, j_1, \cdots i_A, j_A$ are sampled by Metropolis updates, while the auxiliary fields are sampled by the hybrid MC algorithm (see also below). In the left panel of Fig. 1 we show a sketch of the pinhole locations and spin-isospin indices for the operator $\rho_{i_1,j_1,\cdots i_A,j_A}(\mathbf{n}_1,\cdots \mathbf{n}_A)$ inserted at time $t = L_t a_t/2$. We obtain the ground state expectation value by extrapolating to the limit of infinite projection time.

For spatial lattice spacing a, the coordinates $\mathbf{r}_i$ of each nucleon on the lattice is an integer vector $\mathbf{n}_i$ times a. We do not consider mass differences between protons and neutrons for the moment. Since the centre of mass is a mass-weighted average of A nucleons with the same mass, the centre-of-mass position $\mathbf{r}_{\rm CM}$ is an integer vector $\mathbf{n}_{\rm CM}$ times a/A. Therefore the density distribution has a resolution scale that is A times smaller than the lattice spacing. In order to determine the centre-of-mass position $\mathbf{r}_{\rm CM}$, we minimise the squared radius

$$\sum_i |\mathbf{r}_{\rm CM} - \mathbf{r}_i|^2 \tag{7}$$

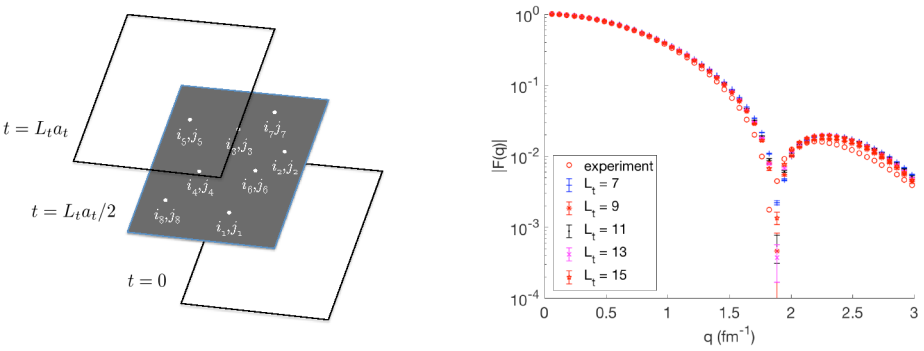

Figure 1. Left panel: A sketch of the pinhole locations and spin-isospin indices $(i_n j_n)$ at time $t = L_t a_t/2$. Right panel: The elastic form factor $F(q)$ for ^{12}C calculated with the pinhole algorithm. Open circles are the experimental values, the other symbols refer to NLEFT results for various Euclidean times L_t.

where each term $|\mathbf{r}_{\rm CM} - \mathbf{r}_i|$ is minimised with respect to all periodic copies of the separation distance on the lattice. As a first application, we show in the right panel of Fig. 1 the calculated elastic form factor of ^{12}C (which is the Fourier transform of the charge density, calculated using the pinhole algorithm[3]). The agreement with the data is quite satisfactory. This paves the way for detailed nuclear structure investigations.

4.2 The Shuttle Algorithm

In most NLEFT simulations, the hybrid MC (HMC) algorithm is used to update the configurations, which consist of nucleon world-lines coupled to external fields. In Ref. 4, we presented the so-called shuttle algorithm. More precisely, the auxiliary fields $s(n_t, \boldsymbol{n})$ that represent the interactions between the nucleons are updated using the shuttle algorithm, where only one time slice is updated at a time. In Fig. 2 a schematic plot sketching the difference between the shuttle algorithm and the HMC algorithm which performs an update of all time slices is shown. The shuttle algorithm works as follows:

1. Choose one time slice n_t, record the corresponding auxiliary field as $s_{\rm old}(n_t, \boldsymbol{n})$.

2. Propose the new auxiliary fields $s_{\rm new}(n_t, \boldsymbol{n})$ at each lattice site $\boldsymbol{n}$ according to the probability distribution $P\left[s_{\rm new}(n_t, \boldsymbol{n}) = \phi_k\right] = \omega_k$ for $k = 1, 2, 3$. We note that $\omega_1 + \omega_2 + \omega_3 = 1$.

3. Calculate the determinant of the $A \times A$ correlation matrix M_{ij} using $s_{\rm old}(n_t, \boldsymbol{n})$ and $s_{\rm new}(n_t, \boldsymbol{n})$, respectively.

4. Generate a random number $r \in [0, 1)$ and perform the following "Metropolis test". If

$$\left| \frac{\det\left[M_{ij}\left(s_{\rm new}(n_t, \boldsymbol{n})\right)\right]}{\det\left[M_{ij}\left(s_{\rm old}(n_t, \boldsymbol{n})\right)\right]} \right| > r \tag{8}$$

accept the new configuration $s_{\rm new}(n_t, \boldsymbol{n})$ and update the wave functions accordingly, otherwise keep $s_{\rm old}(n_t, \boldsymbol{n})$.

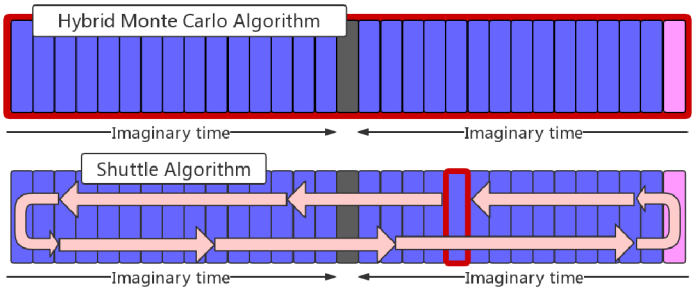

Figure 2. Schematic plot for the HMC algorithm (upper panel) and the shuttle algorithm (lower panel). The red squares denote the time slices to be updated in each run. The pink, blue and black boxes refer to the centre-of-mass projection, the SU(4) invariant transfer matrix and the density operator under consideration, respectively.

5. Proceed to the next time slice, repeat steps 1)-4), and turn around at the end of the time series.

As shown in Fig. 2, the program runs back-and-forth like a shuttle bus and all the auxiliary fields are updated after one cycle is finished. The shuttle algorithm is well suited for small values of the temporal lattice spacing a_t. In this case the number of time slices is large and the impact of a single update is small. In each update the new configuration is close to the old one, resulting in a high acceptance rate. For example, in the recent works discussed below, the temporal lattice spacing is $a_t = 0.001$ MeV^{-1} and the acceptance rate is around 50 % in most cases. We compared the results with the HMC algorithm and found that the new algorithm is more efficient. In most cases the number of independent configurations per hour generated by the shuttle algorithm is three or four times larger than that generated by the HMC algorithm.

4.3 Essential Elements of Nuclear Binding

NLEFT and other *ab initio* methods encounter problems when going to larger mass numbers. More precisely, the three-body forces (and eventually four-body forces) become more important with increasing A, which makes the computations more difficult and harder to control. This led *e. g.* our collaboration to introduce an effective four-nucleon term when considering alpha-type nuclei up to ^{28}Si in 2014.[5] In Ref. 4, we presented a highly improved LO action that overcomes these problems and allows to elucidate the essential mechanisms underlying nuclear binding. For related investigations in the continuum, see *e. g.* Ref. 6 (and references therein).

We start with a simple SU(4)-invariant leading order EFT without explicit pions on a periodic L^3 cube with lattice coordinates $\boldsymbol{n} = (n_x, n_y, n_z)$. The Hamiltonian is

$$H_{\mathrm{SU(4)}} = H_{\mathrm{free}} + \frac{1}{2!}C_2 \sum_{\boldsymbol{n}} \tilde{\rho}(\boldsymbol{n})^2 + \frac{1}{3!}C_3 \sum_{\boldsymbol{n}} \tilde{\rho}(\boldsymbol{n})^3 \tag{9}$$

where H_{free} is the free nucleon Hamiltonian with nucleon mass $m = 938.9$ MeV. The

density operator $\tilde{\rho}(\boldsymbol{n})$ is defined in the same manner as in Ref. 3,

$$\tilde{\rho}(\boldsymbol{n}) = \sum_i \tilde{a}_i^\dagger(\boldsymbol{n})\tilde{a}_i(\boldsymbol{n}) + s_L \sum_{|\boldsymbol{n}'-\boldsymbol{n}|=1} \sum_i \tilde{a}_i^\dagger(\boldsymbol{n}')\tilde{a}_i(\boldsymbol{n}') \tag{10}$$

where i is the joint spin-isospin index and the smeared annihilation and creation operators are defined as

$$\tilde{a}_i(\boldsymbol{n}) = a_i(\boldsymbol{n}) + s_{NL} \sum_{|\boldsymbol{n}'-\boldsymbol{n}|=1} a_i(\boldsymbol{n}') \tag{11}$$

The summation over the spin and isospin implies that the interaction is SU(4) invariant. Note that we perform local (L) as well as non-local smearing (NL). In the latter case, the nucleon creation/annihilation operators are distributed over a lattice point and its six neighbours. The parameter s_L controls the range of the local part of the interaction, while s_{NL} controls the range of the nonlocal (*i. e.* velocity-dependent) part of the interaction. The parameters C_2 and C_3 give the strength of the two-body and three-body interactions, respectively. In what follows, we use a lattice spacing $a = 1.32$ fm, which corresponds to a momentum cutoff $\Lambda = \pi/a \approx 465$ MeV. The dynamics with momentum Q much smaller than Λ can be well described and residual lattice artifacts are suppressed by powers of Q/Λ, see Ref. 7. For systems with more than three nucleons, we use AFMC lattice simulations for a cubic periodic box with length L, see Ref. 2. For nuclei with $A < 30$ nucleons, we take $L \geq 8$, with larger values of L for cases where more accuracy is desired. For nuclei with $A \geq 30$ we take $L = 9$. The temporal lattice spacing is 0.001 MeV^{-1} and the projection time is set to 0.3 MeV^{-1}. We find that these settings are enough to provide accurate results for systems with $A \leq 48$. We also use the recently-developed pinhole algorithm[3] in order to calculate density distributions and charge radii. We use few-body data with $A \leq 3$ to fix the interaction coefficients C_2 and C_3, while the range of the interactions are controlled by the parameters s_{NL} and s_L. In the few-body sector, the two smearing parameters s_{NL} and s_L produce very similar effects and are difficult to distinguish from few-body data alone. Therefore, to pin down s_L and s_{NL} more precisely, we require fits to heavier nuclei as described in detail in Ref. 4. The full set of optimised parameters are $C_2 = -3.41 \times 10^{-7}$ MeV^{-2}, $C_3 = -1.4 \times 10^{-14}$ MeV^{-5}, $s_{NL} = 0.5$, and $s_L = 0.061$.

Using this highly improved action, we have calculated the binding energies for 86 bound even-even nuclei (even number of protons, even number of neutrons) with up to $A = 48$ nucleons, see the left panel of Fig. 3. Due to the SU(4) symmetry, there is no sign problem and all of the MC error bars are smaller than the size of the symbols. The remaining errors due to imaginary time and volume extrapolations are also small, less than 1 % relative error, and thus are also not explicitly shown. The general trends for the binding energies along each isotopic chain are well reproduced. In particular, the isotopic curves on the proton-rich side are close to the experimental results. The discrepancy is somewhat larger on the neutron-rich side and is a sign of missing effects such as spin-dependent interactions. With the same interaction, one can also calculate the charge density profile of a given nucleus. This has been done in Ref. 4 for ^{16}O and ^{40}Ca and the results are quite accurate for such a simple nuclear interaction.

Further, predictions can be made for pure neutron matter (NM), see the right panel of Fig. 3. There, we show the calculated NM energy as a function of the neutron density and the comparison with other calculations using next-to-next-to-next-to-leading-order

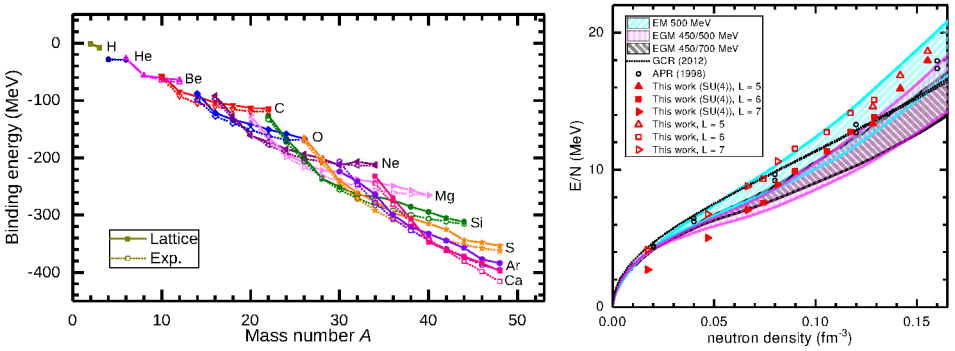

Figure 3. Left panel: The calculated binding energies from ^{3}H to ^{48}Ca. The solid symbols denote the lattice results and the open symbols denote the experimental values. Different symbols and colours denote different elements. The experimental values are taken from Ref. 8. Right panel: The pure neutron matter (NM) energy as a function of neutron density calculated using the NL50[4] interaction with box size L=5 (upright triangles), L=6 (squares), L=7 (rightward-pointing triangles), respectively. The filled red polygons show results for the leading-order SU(4)-symmetric interaction. The open red polygons show an improved calculation with a short-range interaction to reproduce the physical neutron-neutron scattering length as well as a correction to improve invariance under Galilean boosts. For comparison we also show results calculated with full N^{3}LO chiral interactions (EM 500 MeV, EGM 450/500 MeV and EGM 450/700 MeV),[9] the results from variational (APR)[10] and Auxiliary Field Diffusion MC calculations (GCR).[11]

(N^{3}LO) chiral interactions. In the lattice results we vary the number of neutrons from 14 to 66. The data for three different box sizes L=5 (upright triangles), L=6 (squares), L=7 (rightward-pointing triangles) are marked as filled red polygons. We see that our results are in general agreement with the other calculations at densities above 0.05 fm^{-3}, though calculations at higher orders are needed and are planned in future work to estimate uncertainties. At lower densities the discrepancy is larger as a result of the SU(4)-invariant interaction having the incorrect neutron-neutron scattering length. The open red polygons, again L=5 (upright triangles), L=6 (squares), L=7 (rightward-pointing triangles), show an improved calculation with a short-range interaction to reproduce the physical neutron-neutron scattering length as well as a correction to improve invariance under Galilean boosts. The restoration of Galilean invariance on the lattice is described in Ref. 12. Overall, the results are quite good in view of the simplicity of the four-parameter interaction.

The computational effort needed for the auxiliary-field lattice Monte Carlo simulations scales with the number of nucleons, A, as somewhere between A^1 to A^2 for medium mass nuclei. The actual exponent depends on the architecture of the computing platform. The SU(4)-invariant interaction provides an enormous computational advantage by removing sign oscillations from the lattice Monte Carlo simulations for any even-even nucleus. Coulomb interactions and all other corrections can be implemented using perturbation theory or the recently-developed eigenvector continuation method if the corrections are too large for perturbation theory.[13] Given the mild scaling with nucleon number and suppression of sign oscillations, the methods presented here provide a new route to realistic lattice simulations of heavy nuclei in the future with as many as one or two hundred nucleons. By realistic calculations we mean calculations where one can demonstrate order-by-order convergence in the chiral expansion going from LO to NLO, NLO to N^{2}LO, and N^{2}LO to N^{3}LO and so on, while maintaining agreement with empirical data.

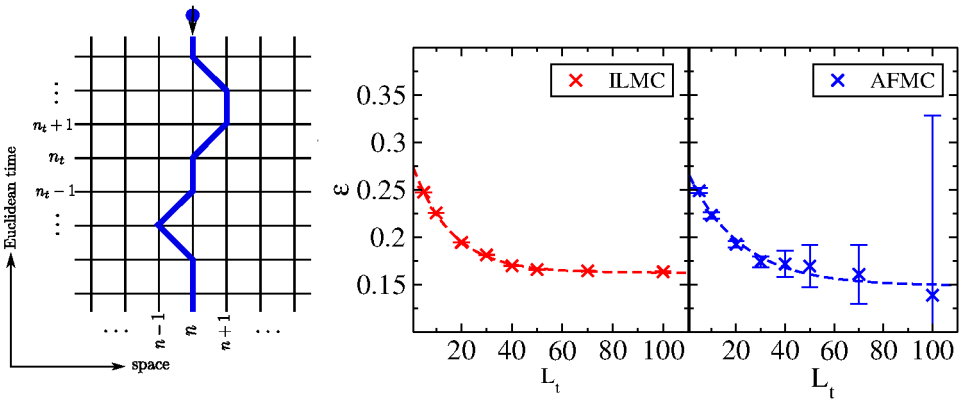

Figure 4. Left panel: A segment of a worldline configuration for a ↓ impurity in a sea of ↑-particles on a 1+1 dimensional Euclidean lattice. Right panel: The ground state energy as a function of Euclidean projection time for ILMC simulations versus AFMC simulations for $L^3 = 10^3$ and $N = 10$.

4.4 Impurity Lattice Monte-Carlo Algorithm and Polaron Physics

Hyper-nuclear (or strangeness nuclear) physics investigates nuclei, in which one (or two) nucleon(s) are substituted by a Λ or Σ hyperon (or two of these). This extends the nuclear chart into a third dimension, because such nuclei are catalogued in terms of proton number Z, neutron number N and strangeness $S = -1, -2, ...$ for one, two, ... hyperons. Such systems are in particular interesting as only very few hyperon-nucleon and hyperon-hyperon scattering data points (~ 50) exist, in contrast to the about 10 000 data on nucleon-nucleon scattering below pion production threshold. This is, of course, a consequence of the fact that no beams of hyperons exist and scattering data can only be inferred from final-state interactions. Therefore, bound systems including hyperons give important information on these elusive baryon-baryon interactions. It should also be noted that hyperon-nucleon scattering lengths are not unnaturally large (as far as they are known), see *e. g.* Ref. 14.

So the question naturally arises how to treat these systems in NLEFT? A first approach is to simply enlarge the degrees of freedom from the nucleon doublet to the hyperons with strangeness $S = -1$. A LO computation using just the contact terms and fitting the low-energy constants to certain cross section threshold ratios showed that such an approach is feasible and the volume dependence of the scattering lengths is consistent with the Lüscher formula.[15] However, due to the missing SU(4) Wigner symmetry in this type of systems, this approach was not further developed. So is there another method to treat hyperons in nuclei? The answer leads us to the so-called *impurity lattice MC algorithm* (ILMC), where the hyperon(s) are treated as an impurity(ies) in a sea of nucleons.

The basic idea of the ILMC algorithm was developed in Ref. 16. Consider a worldline configuration for the impurity as shown in the left panel of Fig. 4 and then compute the reduced transfer matrix by integrating out the impurity. To be specific, consider a system of one ↓-particle in a sea of ↑-particles with $m_\uparrow = m_\downarrow = m$. The lattice Hamiltonian

$H = H_0 + V$ is given by:

$$H_0 = H_0^{\uparrow} + H_0^{\downarrow} \,, \quad V = C_0 \sum_{\vec{n}} \rho_{\uparrow}(\vec{n})\, \rho_{\downarrow}(\vec{n})$$

$$H_0^s = \frac{1}{2m} \sum_{l=1}^{3} \sum_{\vec{n}} \left[2a_s^{\dagger}(\vec{n}) a_s(\vec{n}) - a_s^{\dagger}(\vec{n}) a_s(\vec{n}+\hat{l}) - a_s^{\dagger}(\vec{n}) a_s(\vec{n}-\hat{l}) \right] \tag{12}$$

with $s = \uparrow, \downarrow$, $\hat{l}$ is a unit vector on the lattice and C_0 is tuned to the binding energy of the shallow dimer consisting of one $\uparrow$ and the $\downarrow$-particle. It is advantageous to work in the occupation number basis,

$$\left| \chi_{n_t}^{\uparrow}, \chi_{n_t}^{\downarrow} \right\rangle = \prod_{\vec{n}} \left\{ \left[a_{\uparrow}^{\dagger}(\vec{n}) \right]^{\chi_{n_t}^{\uparrow}(\vec{n})} \left[a_{\downarrow}^{\dagger}(\vec{n}) \right]^{\chi_{n_t}^{\downarrow}(\vec{n})} \right\} \,, \;\; \chi_{n_t}^{s}(\vec{n}) = 0 \text{ or } 1 \tag{13}$$

This allows to calculate the elements of the reduced transfer matrix,

$$\left\langle \chi_{n_t+1}^{\uparrow}, \chi_{n_t+1}^{\downarrow} \right| M \left| \chi_{n_t}^{\uparrow}, \chi_{n_t}^{\downarrow} \right\rangle \tag{14}$$

In computing the transfer matrix, one has to deal with two different cases. First, if the impurity performs one spatial hop,

$$M_{\vec{n}'' \pm \hat{l}, \vec{n}''} = \left(\frac{\alpha_t}{2m} \right) \, : \exp\left[-\alpha_t H_0^{\uparrow} \right] : \tag{15}$$

with $\alpha_t = a_t/a$. If the impurity worldline remains stationary, the corresponding transfer matrix reads

$$M_{\vec{n}'', \vec{n}''} = \left(1 - \frac{3\alpha_t}{m} \right) \, : \exp\left[-\alpha_t H_0^{\uparrow} - \frac{\alpha_t C_0}{1 - 3\alpha_t/m} \rho_{\uparrow}(\vec{n}'') \right] : \tag{16}$$

Note that these reduced transfer matrices are just one-body operators on the linear space of the $\uparrow$-particles. With that, one can proceed as usual in NLEFT.

To show the power of the ILMC, we present in the right panel of Fig. 4 results for the ground state energy of a system of $9\,|\uparrow\rangle + 1\,|\downarrow\rangle$ particles in a volume $L^3 = 10^3$ ($N = 10$) with a zero-range interaction, using both conventional AFMC and the ILMC.[17] The ground state energy ϵ is given by:

$$\epsilon = \frac{1}{a_t} \lim_{L_t \to \infty} \ln \frac{Z(L_t - 1)}{Z(L_t)} \tag{17}$$

The ILMC clearly outperforms AFMC, because it is computationally simpler and faster and also has far smaller sign oscillations (see the detailed discussion in Ref. 17).

As a first application of the ILMC, we considered the polaron problem in two and three dimensions.[17] As a benchmark of the method, we calculated the universal polaron energy in three dimensions (3D) in the scale-invariant unitarity limit and found agreement with published results, see the left panel of Fig. 5. Next, consider attractive polarons in two dimensions. There is a very interesting and important question as to whether a polaron-molecule transition occurs in the ground state as a function of the interaction strength. At present cold-atom experiments are not yet conclusive on the question of a transition. The existence and nature of such a transition impacts the overall phase diagram for spin-imbalanced 2D Fermi gas. The theoretical investigations on this issues were so far inconclusive, see the discussion in Ref. 17. We have investigated this problem considering

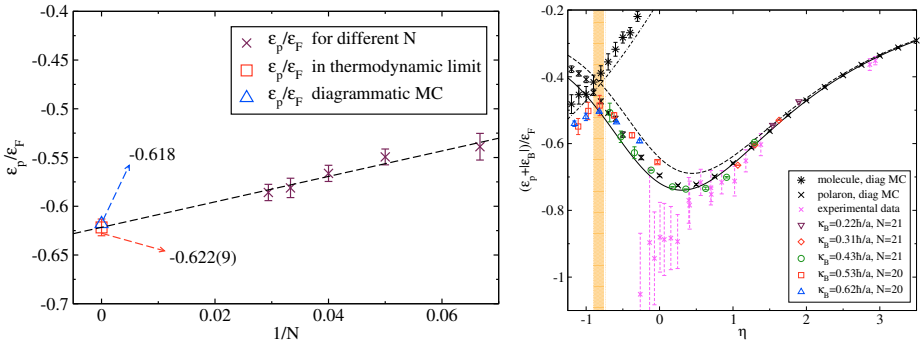

Figure 5. Left panel: The 3D unitarity limit polaron energy ϵ_P in units of the Fermi energy ϵ_F as a function of the inverse particle number $1/N$. The square is the ILMC result in the thermodynamic limit $N \to \infty$, while the triangle gives the diagrammatic Monte Carlo result from Ref. 18. Right panel: Ground state energy as a function of the dimensionless parameter $\eta = (1/2)\ln((2\epsilon_F/|\epsilon_B|))$ in comparison with diagrammatic MC results.[19] The data are from Ref. 20. The vertical band represents the region where the crossover transition from a polaron to a molecule occurs.

again one down-spin impurity and N up-spin particles in the limit of zero-range attractive interactions. The delta function interaction is tuned according to the two-body bound state energy, $|\epsilon_B|$. Using ILMC, we calculated the polaron energy as a fraction of the up-spin Fermi energy. The coupling constant was tuned in order to get the two-body bound states with binding momentum $\kappa_B = \sqrt{m|\epsilon_B|}$ equal to $0.22/a$, $0.31/a$, $0.43/a$, $0.53/a$, and $0.62/a$. We ran simulations for several different lattice areas, L^2, and several different particle numbers, N. The lattice sizes go from $L^2 \times L_t = 20^2 \times 100$ to $L^2 \times L_t = 80^2 \times 700$. For each L^2 and N, the ground state energy was obtained by extrapolating to the limit $L_t \to \infty$ by fitting the Euclidean time projection amplitude to the asymptotic function $\epsilon_0 + \alpha \exp(-\delta \cdot t)$. To magnify the details, we subtracted the dimer energy in vacuum, ϵ_B, from the polaron energies and scaled by ϵ_F, the majority up-spin particle Fermi energy. In Fig. 5 we show the subtracted-scaled polaron energy $(\epsilon_\mathrm{p} + |\epsilon_\mathrm{B}|)/\epsilon_\mathrm{F}$ versus the dimensionless parameter $\eta \equiv \frac{1}{2}\ln\left(\frac{2\epsilon_\mathrm{F}}{|\epsilon_\mathrm{B}|}\right)$, which characterises the strength of the interaction. The simulations are done with $N = 21$ and $N = 20$ up-spin particles. For comparison we have plotted the diagrammatic Monte Carlo results from Ref. 19 and variational results from Ref. 20. We find good agreement with the data in the weak-coupling region, $\eta > 1$. In the very strong coupling limit $\eta \to -\infty$, one expects $(\epsilon_\mathrm{p} + |\epsilon_\mathrm{B}|)/\epsilon_\mathrm{F}$ to approach -1 from above. This corresponds to a tightly-bound molecule that has pulled one up-spin from the Fermi sea and is only weakly repelled by the remaining up spins. Perhaps most interesting is that the lattice results show a smooth dependence on energy in the intermediate region $-0.90 < \eta < -0.75$. We interpret this as evidence for a smooth crossover from fermionic polaron to bosonic molecule. In order to uncover the underlying nature of the polaron-molecule transition, we have used ILMC to measure the density-density correlation function between the impurity and the majority particles. As discussed in Ref. 17, there is no sign of a sharp phase transition such as a divergence of the correlation function or non-analytic dependence on the interaction strength. This shows that the polaron-molecule transition is a smooth crossover. These interesting results clearly show the power of the ILMC and time is ripe now to apply it to the physics of hyper-nuclei.

5 Outlook: What is next?

At this time, NLEFT has matured into a well-established *ab initio* framework at the forefront of the theory of nuclear structure and reactions. The ongoing development of both theory and algorithms is expected to provide further insight into a number of key problems, and to further extend the applicability of NLEFT to heavier nuclei. For example, NLEFT is well placed to address the issues of the mechanism underlying pairing in nuclei, the microscopic origin of the so-important spin-orbit force in nuclei or the precise location of the drip lines of the nuclear chart. A slight modification of the pinhole algorithm, the so-called *trace pinhole algorithm*, allows one to perform first principles calculations in nuclear thermodynamics. Questions of high importance are the precise location of the liquid-gas phase transition in the phase diagram of baryonic matter or the cluster-fragment distribution in the collisions of mid-mass nuclei measured at various facilities world-wide. Scattering processes at stellar energies can also be addressed, in particular the so-called "holy grail" of nuclear astrophysics, *i. e.* the $^{12}\mathrm{C}(\alpha,\gamma)^{16}\mathrm{O}$ reaction at stellar energies, is within reach. In short, NLEFT appears headed towards exciting times of progress and discoveries.

Acknowledgements

I thank my NLEFT colleagues for their contributions to the results presented here. This work is supported in part by the DFG (Grant No. TRR110) through the funds provided to the Sino-German CRC 110 "Symmetries and the Emergence of Structure in QCD", by the Chinese Academy of Sciences (CAS) President's International Fellowship Initiative (PIFI) (grant no. 2018DM0034) and by VolkswagenStiftung (grant no. 93562). The computational resources were provided by the Jülich Supercomputing Centre (JSC) at Forschungszentrum Jülich and by RWTH Aachen.

References

1. E. Epelbaum, H. W. Hammer, and U.-G. Meißner, *Modern Theory of Nuclear Forces*, Rev. Mod. Phys. **81**, 1773, 2009.
2. T. A. Lähde and U.-G. Meißner, *Nuclear Lattice Effective Field Theory : An Introduction*, Lect. Notes Phys. **957**, Springer, 2019.
3. S. Elhatisari *et al.*, *Ab initio Calculations of the Isotopic Dependence of Nuclear Clustering*, Phys. Rev. Lett. **119**, 222505, 2017.
4. B. N. Lu, N. Li, S. Elhatisari, D. Lee, E. Epelbaum, and U.-G. Meißner, *Essential elements for nuclear binding*, Phys. Lett. B **797**, 134863, 2019.
5. T. A. Lähde, E. Epelbaum, H. Krebs, D. Lee, U.-G. Meißner, and G. Rupak, *Lattice Effective Field Theory for Medium-Mass Nuclei*, Phys. Lett. B **732**, 110, 2014.
6. S. König, H. W. Grießhammer, H. W. Hammer, and U. van Kolck, *Nuclear Physics Around the Unitarity Limit*, Phys. Rev. Lett. **118**, 202501, 2017.
7. N. Klein, D. Lee and U.-G. Meißner, *Lattice Improvement in Lattice Effective Field Theory*, Eur. Phys. J. A **54**, 233, 2018.
8. M. Wang *et al.*, *The AME2016 atomic mass evaluation (II). Tables, graphs and references*, Chin. Phys. C **41**, 030003, 2017.

9. I. Tews, T. Krüger, K. Hebeler, and A. Schwenk, *Neutron matter at next-to-next-to-next-to-leading order in chiral effective field theory*, Phys. Rev. Lett. **110**, 032504, 2013.
10. A. Akmal, V. R. Pandharipande, and D. G. Ravenhall, *The Equation of state of nucleon matter and neutron star structure*, Phys. Rev. C **58**, 1804, 1998.
11. S. Gandolfi, J. Carlson, and S. Reddy, *The maximum mass and radius of neutron stars and the nuclear symmetry energy*, Phys. Rev. C **85**, 032801, 2012.
12. N. Li, S. Elhatisari, E. Epelbaum, D. Lee, B. Lu, and U.-G. Meißner, *Galilean invariance restoration on the lattice*, Phys. Rev. C **99**, 064001, 2019.
13. D. Frame, R. He, I. Ipsen, D. Lee, D. Lee, and E. Rrapaj, *Eigenvector continuation with subspace learning*, Phys. Rev. Lett. **121**, 032501, 2018.
14. J. Haidenbauer, U.-G. Meißner, and A. Nogga, *Hyperon-nucleon interaction within chiral effective field theory revisited*, accepted for publication in Eur. Phys. J. A, 2019, arXiv:1906.11681 [nucl-th].
15. S. Bour, Master Thesis, University of Bonn, unpublished (2009).
16. S. Elhatisari and D. Lee, *Fermion-dimer scattering using an impurity lattice Monte Carlo approach and the adiabatic projection method*, Phys. Rev. C **90**, 064001, 2014.
17. S. Bour, D. Lee, H.-W. Hammer, and U.-G. Meißner, *Ab initio Lattice Results for Fermi Polarons in Two Dimensions*, Phys. Rev. Lett. **115**, 185301, 2015.
18. N. V. Prokofev and B. V. Svistunov, *Bold diagrammatic Monte Carlo: A generic sign-problem tolerant technique for polaron models and possibly interacting many-body problems*, Phys. Rev. B **77**, 125101, 2008.
19. J. Vlietinck, J. Ryckebusch, and K. Van Houcke, *Diagrammatic Monte Carlo study of the Fermi polaron in two dimensions*, Phys. Rev. B **89**, 085119, 2014.
20. J. Levinsen and M. M. Parish, *Strongly interacting two-dimensional fermi gases*, in Annu. Rev. Cold At. Mol. **3**, World Scientific, Chapter 1, 2015.